

# Thermo-mechanical compression tests on steel-reinforced concrete-filled steel tubular stub columns with high performance materials

David Medall, Carmen Ibáñez\*, Ana Espinós and Manuel L. Romero

ICITECH, Universitat Politècnica de València, Valencia, Spain

(Received July 28, 2023, Revised November 18, 2023, Accepted November 19, 2023)

**Abstract.** Cost-effective solutions provided by composite construction are gaining popularity which, in turn, promotes the appearance on the market of new types of composite sections that allow not only to take advantage of the synergy of steel and concrete working together at room temperature, but also to improve their behaviour at high temperatures. When combined with high performance materials, significant load-bearing capacities can be achieved even with reduced cross-sectional dimensions. Steel-reinforced concrete-filled steel tubular (SR-CFST) columns are one of these innovative composite sections, where an open steel profile is embedded into a CFST section. Besides the renowned benefits of these typologies at room temperature, the fire protection offered by the surrounding concrete to the inner steel profile, gives them an enhanced fire performance which delays its loss of mechanical capacity in a fire scenario. The experimental evidence on the fire behaviour of SR-CFST columns is still scarce, particularly when combined with high performance materials. However, it is being much needed for the development of specific design provisions that consider the use of the inner steel profile in CFST columns. In this work, a new experimental program on the thermo-mechanical behaviour of SR-CFST columns is presented to extend the available experimental database. Ten SR-CFST stub columns, with circular and square geometries, combining high strength steel and concrete were tested. It was seen that the circular specimens reached higher failure times than the square columns, with the failure time increasing both when high strength steel was used at the embedded steel profile and high strength concrete was used as infill. Finally, different proposals for the reduction coefficients of high performance materials were assessed in the prediction of the cross-sectional fire resistance of the SR-CFST columns.

**Keywords:** concrete-filled steel tubular columns; embedded steel profile; fire reduction factors; fire resistance; high strength concrete; high strength steel

## 1. Introduction

The use of high performance materials (i.e., high strength steel and high strength concrete) in composite sections allows to achieve a significant load bearing capacity with reduced cross-sectional dimensions. Given the increased popularity of composite construction all over the world, technological developments in this field are constant and are allowing the appearance of new types of composite sections. With these innovative sections, the benefits of steel and concrete working together are still exploited but, at the same time, improvements are made in other aspects. This is the case of the so-called steel-reinforced concrete-filled steel tubular (SR-CFST) columns, where an open steel profile is embedded into a CFST section. Apart from the well-known advantages of these typologies at room temperature, they show an enhanced fire performance due to the inherent fire protection offered by the surrounding concrete to the inner steel profile, which delays its loss of mechanical capacity at elevated temperatures (Espinós *et al.* 2016). Hence, combined with high performance materials, the column may resist the

applied load for an extended fire exposure time.

In light of the review of the experimental programmes published in the literature, it can be seen that the number of available fire test results on SR-CFST columns is still limited. One of the first works published on SR-CFST columns exposed to fire conditions were the tests performed at the University of Liège by Dotreppe *et al.* (2010). Using self-compacting concrete as infill, the fire resistance of ten slender composite columns was tested. Circular and square shapes for the outer steel tube were combined. Only four of the ten sections were SR-CFST (with an embedded HEB120 steel profile). For a load level of 0.4 and a maximum external dimension of 219.1 mm, the fire resistance times ranged from 39 up to 79 min thanks to the application of intumescent paint in some specimens.

The experiments carried out in Shanghai (Meng *et al.* 2020, 2021) revealed that the inner steel profile considerably enhanced the fire behaviour of the specimens, exceeding 240 min in some cases. The fire resistance of eight SR-CFST columns was tested considering the effect of non-uniform heating in both square and circular geometries. The SR-CFST columns had an embedded HW150 × 150 and a length of 1800 mm although only the central 1200 mm were heated.

More recently, and particularly on SR-CFST columns with a cruciform steel section embedded in the concrete, experiments were conducted at Southeast University (Mao

---

\*Corresponding author, Lecturer  
E-mail: caribus@upv.es

*et al.* 2021, 2022, 2023). In those experiments the columns were tested subjected to uniform and non-uniform heating and with and without fire protection. Once again, circular and square specimens were tested under the ISO-834 standard fire curve and different load ratios. Although high performance materials were not used, it was found that the fire resistance of SR-CFST columns had substantial improvement compared with CFST columns.

The lack of experiments on SR-CFST columns with innovative materials at elevated temperatures was also pointed out by Tan *et al.* (2019a, 2019b) in their works on SR-CFST columns with stainless steel. The authors focused their research on the FE analysis of these columns but the validation of the models was accomplished by parts using experiments on CFST columns with stainless steel since there are not available test data in the published literature that can be used to that end.

With the aim of extending the available experimental data, and based on the conclusions from previous research, this work presents a series of thermo-mechanical tests performed on stub SR-CFST columns. New features, which have not been investigated in the previous experimental campaigns, such as the use of high strength steel (with yield strength over 460 MPa) for the embedded profile and high strength concrete (with cylinder compressive strength over 50 MPa) as infill are covered here to ease the understanding of the performance of these columns in a fire situation. The history of sectional temperatures is analysed as well as the response in terms of axial load–displacement. In total ten SR-CFST stub columns with high performance materials are tested, four circular and six square sections. The test results are analysed and the influence of the high performance materials in the failure times of the columns under fire are evaluated by means of the High Performance Ratio. Finally, the suitable reduction factors for the materials are assessed with a proposed design equation for the evaluation of the load bearing capacity of SR-CFST stub columns at elevated temperatures.

## 2. Experimental program

### 2.1 Definition of tests specimens

Within the framework of this research, in total 12 stub columns were tested under compression at elevated temperatures, combining circular and square shapes. Two of the columns were a circular and square hollow tubes which served as reference and ten were SR-CFST specimens grouped into two series comprising circular and square geometries respectively (see Fig. 1).

The cross-sectional properties of all tested specimens and more data related to each series are summarized in Table 1. For clarity, the test specimens were named as follows: SR-CFST-**X-TM***i* (i.e., SR-CFST-C-TM1), where **X** stands for the cross-sectional shape of the outer steel tube (**C** for circular and **S** for square), **TM** stands for “Thermo-Mechanical” and **i** represents the number of test, each of them with a different combination of grades for the embedded steel profile and the concrete infill. For the

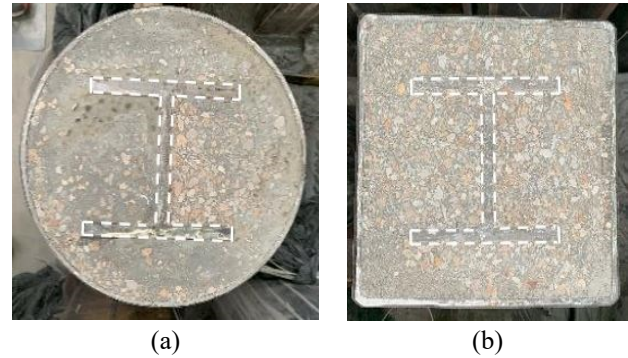


Fig. 1 SR-CFST shapes tested: (a) circular; (b) square

hollow steel tube tests, designation CHS and SHS followed by the label TM0 indicative of a reference case was used

For the circular columns,  $\phi 273 \times 6.3$  mm hollow steel tubes were used for all the specimens, from C-TM0 to C-TM4. For the square specimens, S-TM0 to S-TM4, the selected hollow steel tubes were  $\#220 \times 6.3$  mm, in an intent that the steel usage of the two groups of circular and square specimens was very similar, with a difference of only 0.57% in terms of outer steel tube area. Normal and high strength steel for the embedded profile and also normal and high strength concrete for the infill were combined. As an addition to the square series, specimens S-TM5 and S-TM6 in particular had a  $\#250 \times 10$  mm hollow tube made of high strength steel. The results from these last two test specimens will serve to assess the effect of increasing both the thickness and the strength of the outer steel tube. For the embedded steel profiles, HEB140 sections were used in all the cases, with dimensions  $h=b=140$  mm ( $t_f=12$  mm,  $t_w=7$  mm). All the columns had a length of 600 mm.

### 2.2 Material properties

#### Steel

In this experimental program, cold-formed hollow steel tubes with grade S355 were used for specimens TM0 to TM4. For square specimens TM5 and TM6, hot-rolled quenched and tempered hollow steel tubes with steel grade S770 were used. Regarding the embedded steel profiles, in five of the SR-CFST columns hot-rolled sections with steel grade S275 were used, while for the other five SR-CFST columns, the inner profiles were fabricated from welded high strength steel plates of grade S700MC. For all the hollow steel tubes and embedded steel profiles, the actual values of the yield strength ( $f_{y0}$  and  $f_{yi}$ , respectively) and the ultimate strength ( $f_{u0}$  and  $f_{ui}$ , respectively) were determined through the corresponding coupon tests (three coupons per sample), the average measured value being shown in Table 1.

#### Concrete

Normal and high strength concrete mixes of 30 and 90 MPa characteristic cylinder compressive strength, respectively, were prepared in a planetary mixer and cured in standard conditions for 28 days at the laboratories of the Concrete Science and Technology Institute (ICITECH), Universitat Politècnica de València, using the experience

Table 1 Details of the tested specimens

Specimen	$D$ or $B$ (mm)	$t_o$ (mm)	$f_{yo}$ (MPa)	$f_{uo}$ (MPa)	$f_{yi}$ (MPa)	$f_{ui}$ (MPa)	$f_c$ (MPa)	Moisture (%)	$\mu$ (%)	$N_{exp}$ (kN)	FT (min)
CHS-TM0	273	6.3	413.33	483.28	-	-	-		40	1020.7	63
SR-CFST-C-TM1	273	6.3	413.33	483.28	315	441	29.73	6.28	40	2812.3	267
SR-CFST-C-TM2	273	6.3	413.33	483.28	777.2	853.68	29.73	6.28	40	3488.9	405
SR-CFST-C-TM3	273	6.3	413.33	483.28	315	441	86.16	2.11	40	3936.8	317
SR-CFST-C-TM4	273	6.3	413.33	483.28	777.2	853.68	86.16	2.11	40	4624.3	383
SHS-TM0	220	6.3	495.84	549.65	-	-	-		40	1154.3	43
SR-CFST-S-TM1	220	6.3	495.84	549.65	315	441	29.73	6.28	40	2377.4	239
SR-CFST-S-TM2	220	6.3	495.84	549.65	777.2	853.68	29.73	6.28	40	3097.9	308
SR-CFST-S-TM3	220	6.3	495.84	549.65	315	441	86.16	2.11	40	3306.5	285
SR-CFST-S-TM4	220	6.3	495.84	549.65	777.2	853.68	86.16	2.11	40	4027.0	294
SR-CFST-S-TM5	250	10	824	864	315	441	29.73	6.28	30	3406.5	274
SR-CFST-S-TM6	250	10	824	864	777.2	853.68	86.16	2.11	30	4821.7	395

\*Note:  $D$  and  $B$  are the outer diameter or dimension for circular and square sections respectively;  $t_o$  is the outer steel tube thickness;  $f_{yo}$  and  $f_{yi}$  are the yield strength of steel for the outer steel tube and inner embedded section respectively;  $f_{uo}$  and  $f_{ui}$  are the ultimate strength of steel for the outer steel tube and inner embedded section respectively;  $f_c$  is the concrete cylinder compressive strength;  $\mu$  is the load level;  $N_{exp}$  is the applied load; and FT is the failure time.

acquired in precious experimental campaigns with high strength concrete (Pons *et al.* 2018).

Sets of three cylindrical and three cubic samples for each type of concrete mix used for filling the column specimens were also prepared. Before the start of the experimental program, the pertinent uniaxial compression tests were performed in order to obtain the actual concrete compressive strength ( $f_c$ ), which is given in Table 1. The moisture content values displayed in the same table were obtained for the different concrete batches by following a standard procedure, according to ISO 12570:2000 (ISO 2000). Before drying, the concrete samples obtained from each batch were weighed and afterwards introduced inside a heat chamber for drying at a constant temperature of 105 °C. After 48 h, the samples were extracted from the chamber and let to cool down until reaching 30-40 °C (to minimise re-absorption of moisture) and weighed again until the change of mass was less than 0.1% of the total mass. The moisture content mass by mass was then obtained by relating the mass difference of the test specimen before and after drying to the final mass value.

### 2.3 Specimens preparation

In this experimental campaign, all the columns were prepared and tested at the Concrete Science and Technology Institute (ICITECH), at Universitat Politècnica de València (Spain). At both ends of each specimen, steel plates with dimensions 300 × 300 × 10 mm were placed to ensure that the load application conditions were optimal. The steel plate at the bottom of the embedded steel profile was the first one to be welded (Fig. 2(a)). Before placing the hollow steel tube concentrically with the embedded steel profile, a hole was drilled at the lower part of the steel tube to allow vapour ventilation during heating. This hole was then also used to allow the wires of the thermocouples to pass

through once they were positioned at the cross-section (Fig. 2(b)). Next, the bottom of the hollow steel tube was welded to the steel plate (Fig. 2(c)). Once the column was filled with concrete and it was settled with the help of a needle vibrator, the specimen was covered with a plastic film. Finally, once the top surface was smooth to guarantee planarity and the contact of the steel plate with all the components, the second plate was welded to the top end of the column. Figs. 3-5 show the cross-sections of all the tested specimens.

In Fig. 6 the layout of the set of ten thermocouples positioned at the mid-length of the column is presented. In order to register the complete evolution of the cross-sectional temperatures during the tests, the thermocouples were placed as described next. In the steel components the arrangement was as follows: to the outer steel tube surface, thermocouples number 1 and 6 were welded; and thermocouples number 7, 8, 9 and 10 were welded at different points of the embedded steel profile. At the concrete infill, thermocouples were distributed so that thermocouples number 2, 3 and 4 were placed equidistantly, with a separation of 1/6 of the section width, being thermocouple number 4 in contact with the web of the embedded steel profile. Thermocouple number 5 was also embedded and positioned at 1/4 of the section width.

### 2.4 Test setup and procedure

For the experiments, a thermo-mechanical testing protocol was designed, where a sustained load was applied to the stub SR-CFST columns, being simultaneously heated inside an electrical furnace. For that purpose, a vertical testing frame equipped with a hydraulic jack of 5000 kN capacity was employed as shown in Fig. 7. The applied load was calculated as a 40% of the theoretical ultimate capacity of the columns at room temperature, using the measured

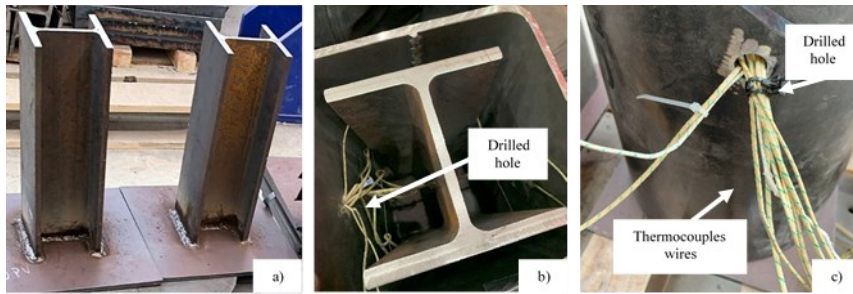


Fig. 2 Columns preparation: a) Steel plate welded at bottom end of the embedded profile; b) Positioning of thermocouples; c) Positioning of hollow steel tube

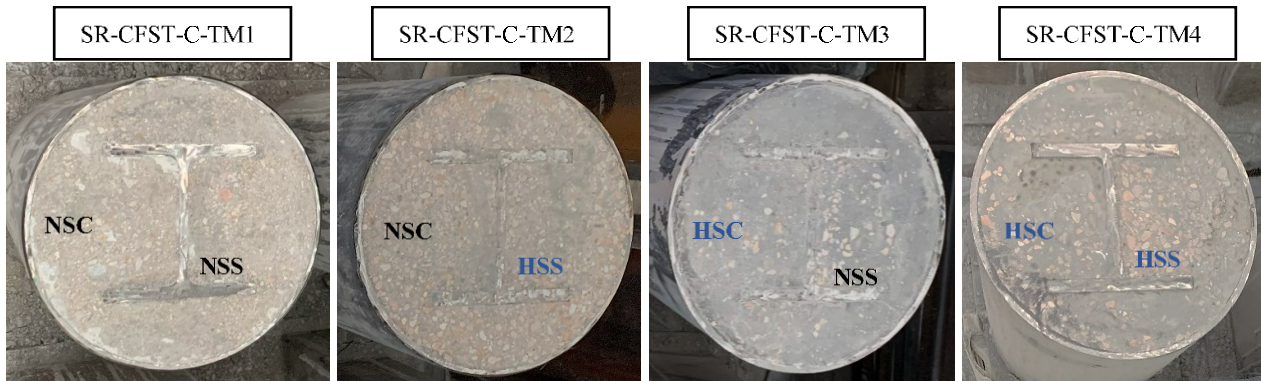


Fig. 3 Circular specimens  $\phi 273 \times 6.3$  mm

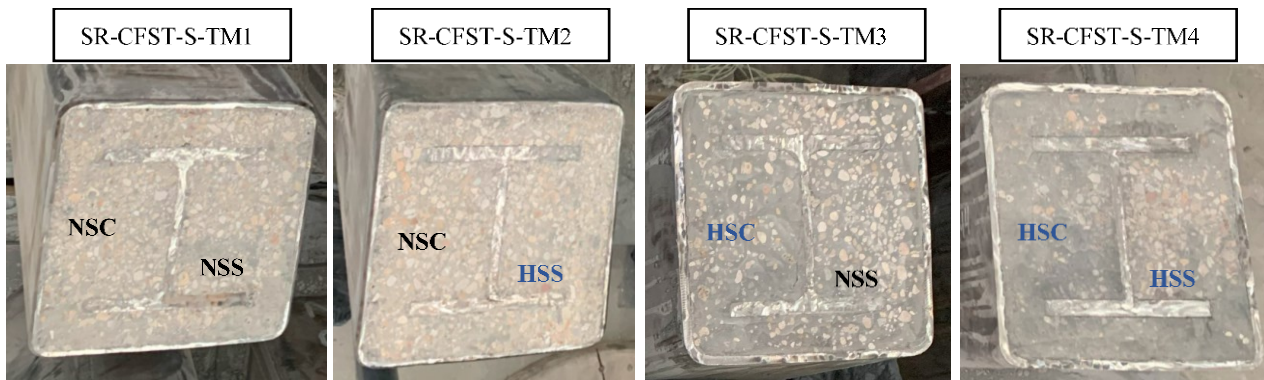


Fig. 4 Square specimens  $\#220 \times 6.3$  mm

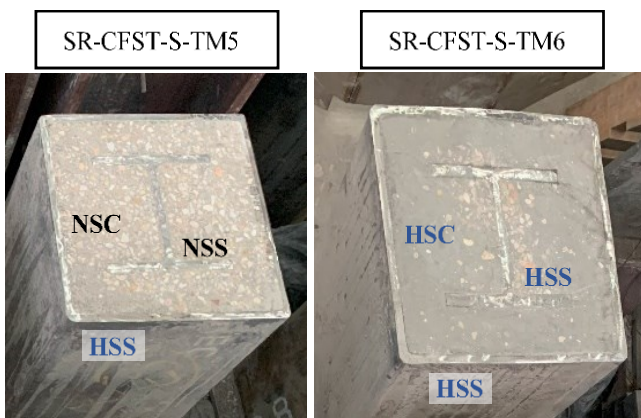


Fig. 5 Square specimens  $\#250 \times 10$  mm (Note: NSC and HSC stand for Normal and High Strength Concrete respectively; NSS and HSS stand for Normal and High Strength Steel respectively)

material strengths, except for specimens S-TM5 and S-TM6, which presented a higher ultimate load, and thus a 30% load level was applied to them, in order not to exceed the capacity of the hydraulic jack, see values of load level ( $\mu$ ) and applied load ( $N_{exp}$ ) in Table 1.

The ultimate capacity of the columns at room temperature necessary to obtain the applied load value was calculated as given in Clause 6.7.3.2 of EN1994-1-1 (CEN 2004) by adding the plastic resistances of the three components of the cross-section (i.e., outer steel tube, concrete infill and inner steel profile).

The load was applied concentrically to the top end of the columns through a spherical bearing, while the bottom end of the columns was attached to the testing rig through a bolted plate. Once the desired load was applied, it was kept constant and the heating of the specimen started, with unrestrained column elongation.

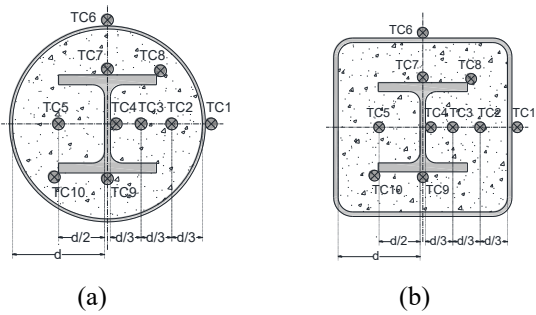


Fig. 6 Layout of thermocouples: a) circular sections; b) square sections

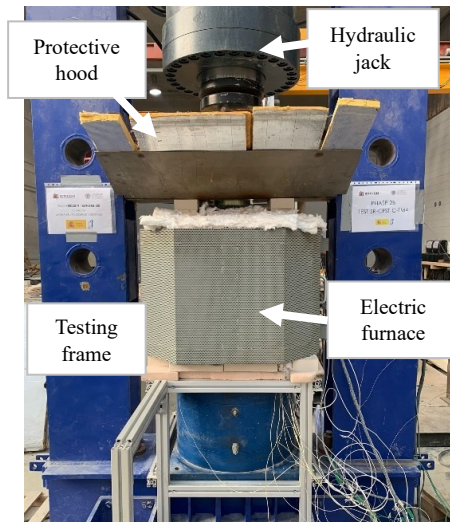


Fig. 7 General view of the test setup

For the heating of the column specimens, an *ad-hoc* manufactured electric furnace of 10000 W power was coupled to the testing rig, see Fig. 7. The furnace had an inner diameter of  $\phi 400$  mm, consisting of two semicylinders joined by a hinge. As can be seen in Fig. 8, the electric elements of the refractory wall of each semicylinder were distributed evenly in parallel layers through the whole length for both sides. To guarantee the uniformity of the heating through measurements of the furnace inner temperature, three thermocouples were evenly distributed inside the furnace chamber along its height.

Fibre blanket was used to cover the open cavities at the top and bottom ends of the furnace once the furnace was closed and the specimen was ready for testing, in order to minimise the heat loss. As can be also seen in Fig. 7, a purpose-made protective hood was attached to the top end of the column to prevent the load cell from receiving the convective heat flow. Additionally, the contacting plates at the top end of the column were thermally insulated with layers of fibre blanket to avoid the possible heat conduction towards the load cell.

A transient heating regime was applied in the thermo-mechanical tests, with a non-constant heating rate. The electric furnace power target was set to its maximum according to the manufacturer specifications, although due to its high inertia at the first stages of heating and the massive size of the tested stub column specimens, the

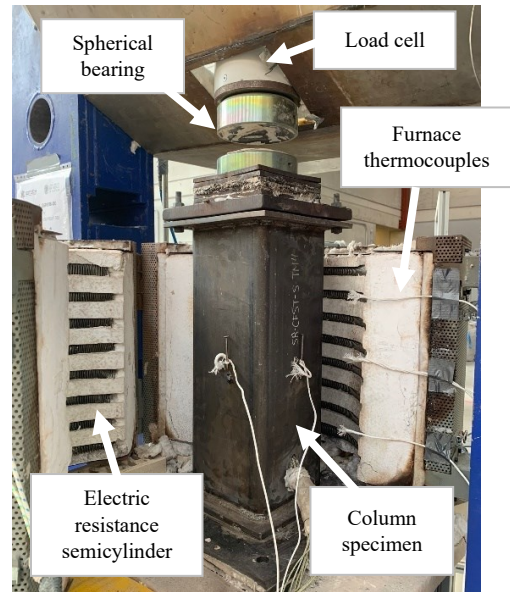
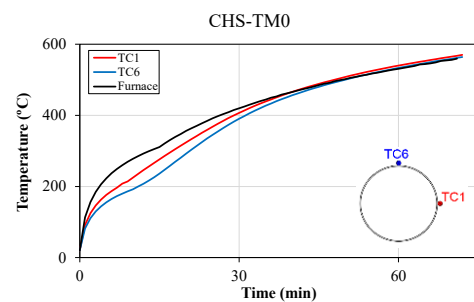
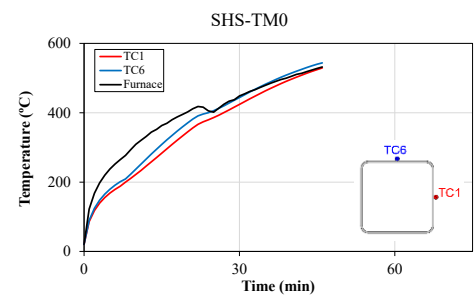


Fig. 8 Specimen prepared for testing inside the electric furnace



(a)



(b)

Fig. 9 Cross-sectional temperatures for hollow specimens CHS-TM0 (a) and SHS-TM0 (b)

standard ISO-834 temperature-time curve was not followed in the tests. This fact justifies that all the comparisons and discussion of results presented in this work refers to “failure times”, rather than “standard fire resistance times”.

### 3. Analysis of test results

#### 3.1 Cross-sectional temperatures

In Figs. 9-11 the evolution of the cross-sectional

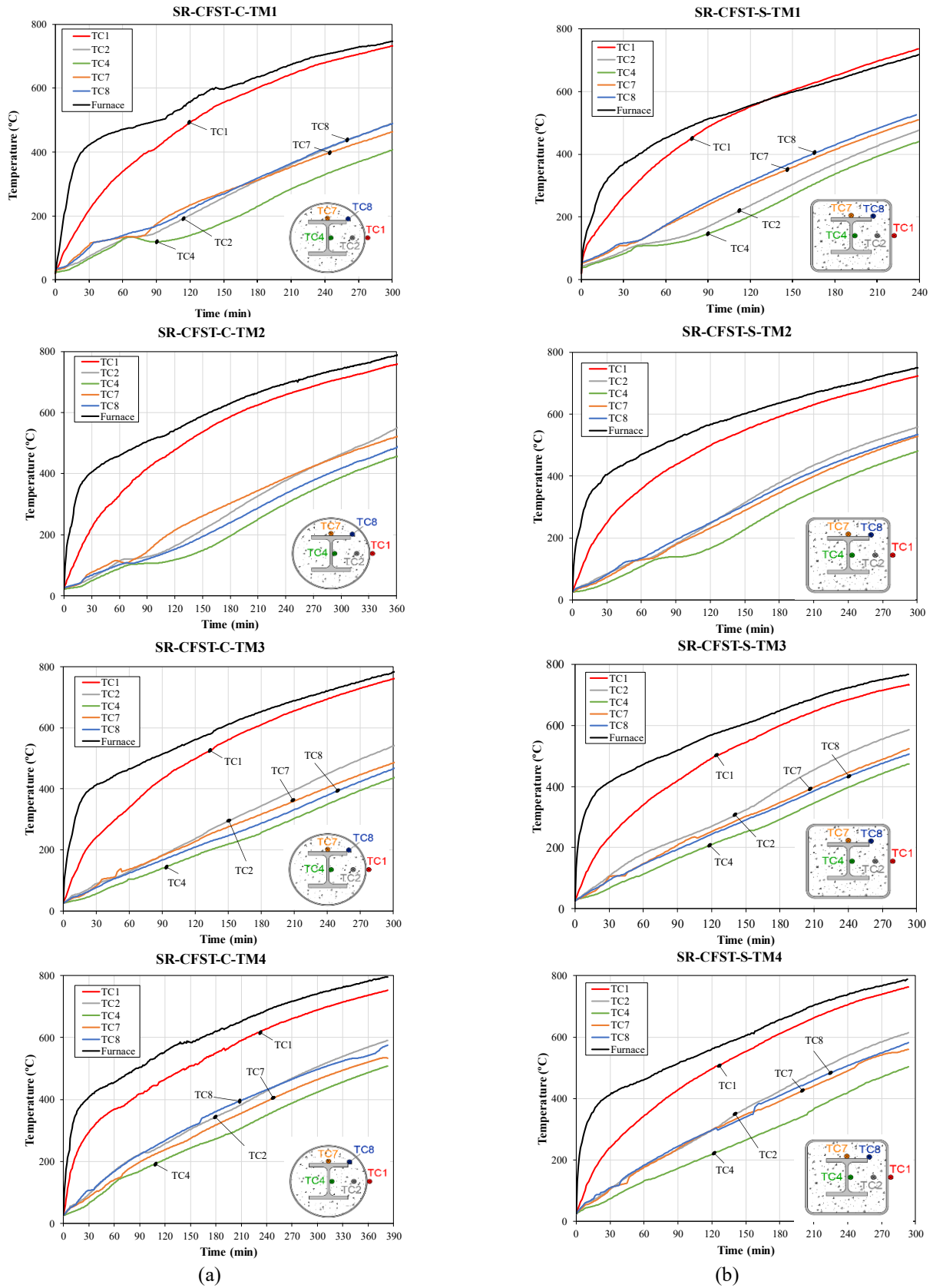


Fig. 10 Cross-sectional temperatures for specimens TM1-TM4; a) circular sections; b) square sections

temperatures is shown for the tested columns but, for the sake of clarity only the data of five of the thermocouples are displayed together with the evolution of the furnace

temperature.

For circular and square specimens of series TM1-TM4 the registered temperatures during the heating process are

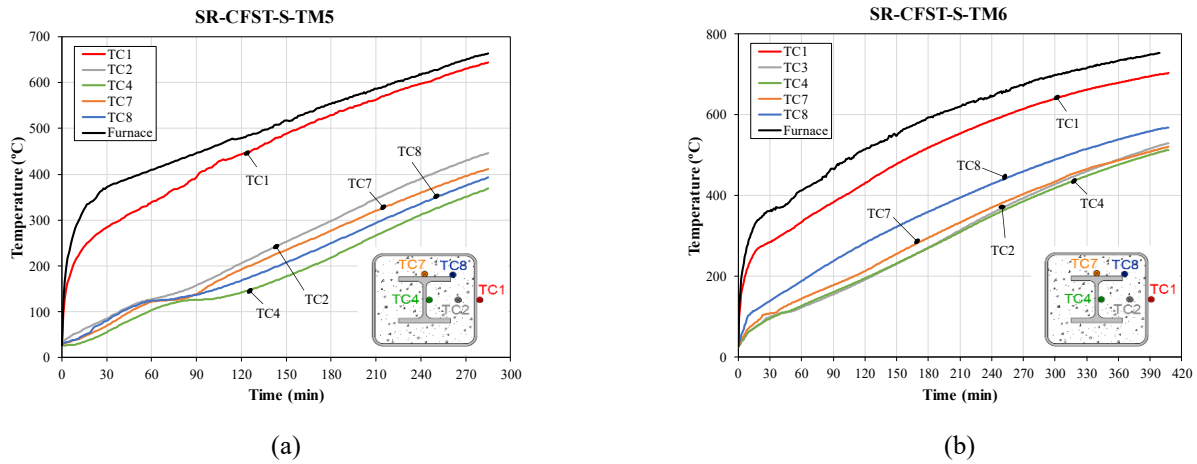


Fig. 11 Cross-sectional temperatures for square specimens S-TM5 (a) and S-TM6 (b)

shown in Fig. 10. For the square SR-CFST columns temperatures were generally higher than for the corresponding circular columns, which may be explained with the effect of the section factor, i.e., for the same cross-sectional area, the square sections present a higher exposed perimeter. For both geometries, the delay of temperature rise at the inner steel profile can be observed. The thermal protection provided by the outer steel tube together with the low thermal diffusivity of concrete are responsible for this effect. In Fig. 9 the evolution of the outer steel tube temperatures is shown for specimens CHS-TM0 and SHS-TM0. In comparison with the composite columns with concrete core and embedded steel profile, it is clear that the steel tube heats much quicker leading to much higher temperatures. For example, in the CHS-TM0, at 30 min the steel tube has achieved 400°C, whereas in the SR-CSFT-C series, it is almost after 90 min of heating when this temperature is reached. The same happens with the SHS-TM0 specimen and the SR-CFST-S series.

In Fig. 11 the history of temperatures at cross-section is shown for square specimens SR-CFST-S-TM5 and SR-CFST-S-TM6, which have a #250x10 mm outer tube made of high strength steel. Both the increase in the sectional dimension and the increase in the outer steel tube thickness evidence much more the delay in the heating of the inner concrete and embedded steel profile. Once more, the outer steel tube provides an inherent thermal protection, enhanced by the increment in the tube thickness (10 mm vs. 6.3 mm).

### 3.2 Failure modes

In Figs. 12-13 photographs of the state of all the columns after the thermo-mechanical tests are displayed. As shown in these figures, the outer steel tubes experienced local buckling around their mid-sections, which was more evident for the hollow tubes. In the SR-CFST columns, the local buckling was more notable for the square specimens.

In Figs. 14-15, the graphs show the evolution along the heating time of the axial displacement at the top end of the column for all the tested columns which was monitored and recorded by means of the load cell, showing a first stage dominated by the expansion of the outer tube; a second



Fig. 12 Hollow columns after the tests

stage with a gradual shortening of the column after the degradation of the outer tube; and the end of the test when eventually the defined failure criterion is met.

Based on EN1363-1 Section 11.1(b) (CEN 2020), a homogenous criterion was defined for determining the failure time of the columns where, for vertical members in compression, failure is established when one of the following two criteria is met:

- Vertical contraction limit:  $h/100$  mm
- Contraction velocity limit:  $3h/1000$  mm

where  $h$  is the initial length of the column. Therefore, the maximum contraction allowed for the tested columns was set to  $600/100=6$  mm and the maximum contraction velocity was set to  $3 \times 600/1000=1.8$  mm/min. For all the SR-CFST tests, the first criterion was met earlier, while for the hollow tube tests, the second criterion was reached sooner.

From the graphs of Figs. 14-15 the evolution of the response can be analysed. At the first stage of the heating, due to the direct exposure to the heat source and the higher thermal expansion of steel as compared to the concrete infill, the outer steel tube supports alone the applied load for a certain amount of time until yielding. After its loss of capacity, the load is transferred to the inner parts of the section, which owing to the higher thermal capacity of the concrete infill, heat up slower and are in turn able to sustain the load for a significant period of time, until

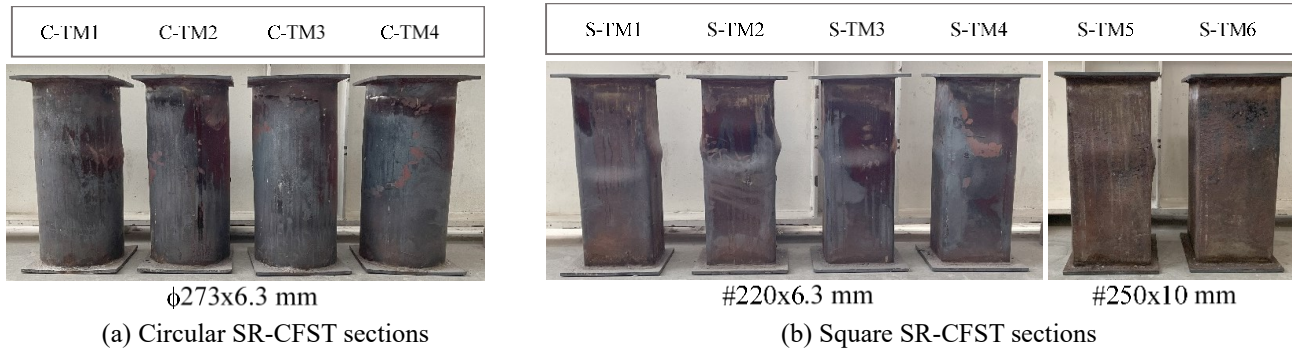


Fig. 13 SR-CFST stub columns after the tests

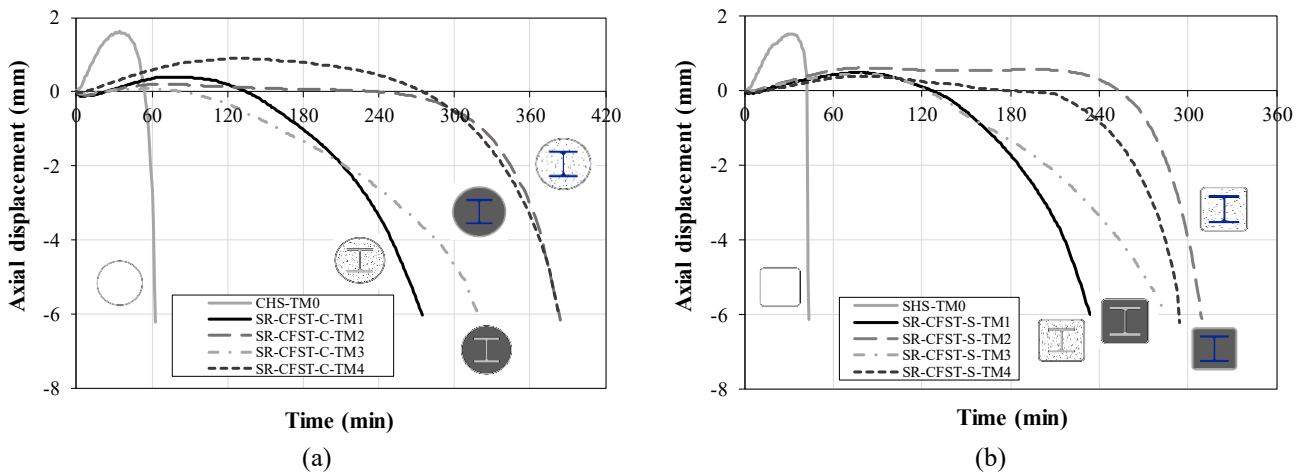


Fig. 14 Axial displacement versus time curves for specimens TM0-TM4 : (a) circular sections; (b) square sections

eventually the degradation of concrete and the inner steel profile occurs, stage where the column axial displacement gradually decreases, as a sign of capacity loss.

### 3.3 Comparison of the thermo-mechanical performance of the different cases analysed

In general, the circular SR-CFST specimens were able to sustain the applied load for a longer heating time than their square counterparts. For each series TM0-TM4, the failure time significantly increased when using high strength steel at the inner profile, and a certain enhancement was also obtained with the use of high strength concrete (HSC).

A much lower failure time was observed for the hollow tubes than for the SR-CFST columns. Their premature failure is due not only to the reduced mechanical capacity triggered by the local buckling of the tube wall, but also to the extremely fast heating of the section. Given the lack of concrete filling, the phenomenon of heat dissipation that benefits the SR-CFST columns does not occur, leading to the sharp increase of temperatures in the steel tube that can be perceived in Fig. 10.

Special mention should be made of the response observed for specimens SR-CFST-S-TM5 and SR-CFST-S-TM6. These specimens have bigger dimensions than their counterparts of the square series and also, the thickness of the steel tube is higher (10 mm vs. 6.3 mm). Although the

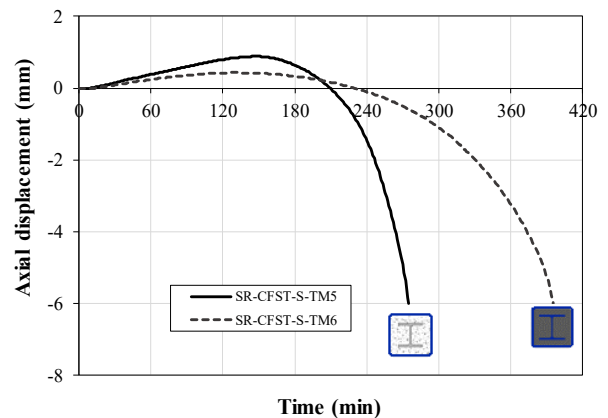


Fig. 15 Axial displacement versus time curves for specimens S-TM5 and S-TM6

failure times (FT) registered were higher, these are lower than expected, even more considering that in these cases high strength steel was used in the outer tube. FT for specimens SR-CFST-S-TM1 and SR-CFST-S-TM4 were 239 min and 294 min correspondingly whereas columns SR-CFST-S-TM5 and SR-CFST-S-TM6 reached 275 and 396 min respectively. As observed previously in Fig. 11, the heating is delayed but the limited improvement leads to think that the outer steel tube acts only as a thermal barrier. It degrades with high temperatures protecting the inner parts

but, at the same time, this does not allow to take advantage of its potential as a high performance material.

This tendency for composite columns with two steel components was already observed by the authors (Romero *et al.* 2015) after conducting a series of tests on double-tube concrete-filled steel tubular columns (DT-CFST) under fire. One of the main conclusions drawn was that in case of fire, a good design strategy for composite columns could be placing the highest amount of steel at the inner part of the section, so as to be thermally protected. Specifically, for SR-CFST this fact was also observed by the authors in a numerical study (Medall *et al.* 2022).

#### 4. Assessment of the failure time of SR-CFST stub columns under fire

In this section, an analysis of the mechanical contribution of the different configurations of materials obtained from the experimental results is conducted. By means of this analysis one of the objectives of this work would be covered: the assessment of the influence that the high performance materials have on the failure time of the SR-CFST columns.

In the investigations related to CFST columns it is common to talk about ratios when conducting these analyses. Thus, taking as a basis the same concept, a new mechanical ratio can be defined: the high performance ratio (HPR).

Considering that the expected enhanced mechanical behaviour of a SR-CFST column with high performance materials with respect to a SR-CFST column with normal strength materials is due precisely to the presence of high strength concrete or high strength steel, the HPR is calculated as the ratio between the failure time achieved by a column of each series ( $FT_{C-TM_i}$  or  $FT_{S-TM_i}$ ) with respect to the failure time measured for the TM1 column of the corresponding series, which will serve as reference ( $FT_{C-TM1}$  or  $FT_{S-TM1}$ ). Therefore, a value greater than unity means that the contribution of the high performance materials is positive. The HPR ratio will be calculated only for specimens TM2 to TM4, both circular and square, since are the ones that have the same cross-sectional area of steel as the corresponding specimen TM1.

For circular SR-CFST columns, Eq. (1) will be used:

$$HPR_{Ci} = \frac{FT_{C-TM_i}}{FT_{C-TM1}} \quad (1)$$

And for square SR-CFST columns, Eq. (2) will apply:

$$HPR_{Si} = \frac{FT_{S-TM_i}}{FT_{S-TM1}} \quad (2)$$

The values obtained for this ratio may help to quantify the trend observed previously through the load-deflection curves. The HPR values are shown in Table 2 and represented in Fig. 16.

In view of the values of the HPR, it is clear that using high strength steel in the inner steel section is the most effective strategy to enhance the fire response of SR-CFST stub columns, especially in circular columns. This may be explained because the circular shape offers the columns a

Table 2 HPR for the different tested specimens

Specimen	FT (min)	HPR
SR-CFST-C-TM1	267	-
SR-CFST-C-TM2	405	1.52
SR-CFST-C-TM3	317	1.19
SR-CFST-C-TM4	383	1.43
SR-CFST-S-TM1	239	-
SR-CFST-S-TM2	308	1.29
SR-CFST-S-TM3	285	1.19
SR-CFST-S-TM4	294	1.23

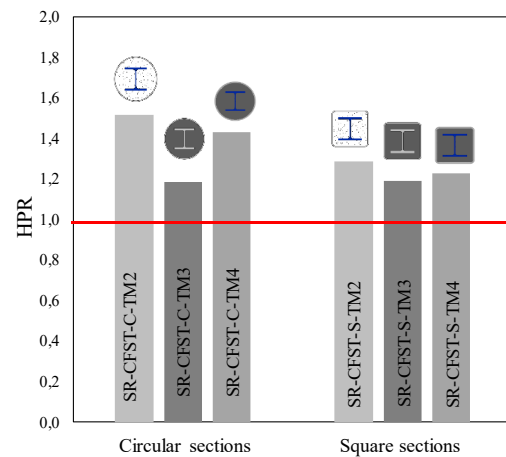


Fig. 16 HPR for both series of tested SR-CFST columns

better thermal behaviour (lower section factor) and also, due to the effect of partial confinement, which should be confirmed by means of further numerical investigations.

However, in both TM3 specimens, the response is mainly controlled by the concrete infill, highly influenced by its moisture content, which according to the measured values was slightly lower for the high strength concrete mixture as compared to the normal strength one, therefore producing a faster heating of the section. Note that with the same moisture content the benefits of filling the SR-CFST columns with high strength concrete would have been even more notable.

For square specimens SR-CFST-S-TM5 and SR-CFST-S-TM6, which had high strength steel outer tubes, improvement ratios had been calculated with respect to specimens SR-CFST-S-TM1 and SR-CFST-S-TM4, which had the same combination of materials for the inner components, i.e., normal strength concrete and steel for the concrete infill and the embedded steel profile respectively in specimen SR-CFST-S-TM1; and high strength concrete and steel in the case of specimen SR-CFST-S-TM4.

Note that specimens S-TM5 and S-TM6 have an increment of 76.38% in the cross-sectional area of steel and 25.53% in the cross-sectional area of concrete. The improvement ratios obtained for each pair are 1.15 for S-TM5 vs. S-TM1 and 1.35 for S-TM6 vs. S-TM4. Considering the greater section dimensions of specimens S-TM5 and S-TM6 and the lower load level applied to them

(30% vs. 40%), the enhancement in terms of failure time obtained by using high strength steel at the outer tube is lower than expected. This corroborates the concept that using more area of steel of a higher grade at the outer tube does not lead to a notable gain in the fire performance of these type of composite columns.

## 5. Assessment of the reduction factors of high-performance materials for SR-CFST stub columns

This section evaluates the current design provisions for the cross-sectional plastic resistance of SR-CFST columns at elevated temperatures and the applicability of the currently available proposed reduction coefficients. These coefficients are taken from international codes as well as from the proposals of different authors. Their accuracy for estimating the cross-sectional plastic resistance of SR-CFST columns under high temperatures is obtained by comparing their predictions with the values registered during the described experiments.

### 5.1 HSS reduction coefficients

Currently, only few design codes incorporate reduction coefficients specifically developed for high strength steels in fire conditions. In the case of EN1993-1-2 (CEN 2005), although the scope of application is limited to steel grades up to S460, it is stated in Clause 2.2 of EN1993-1-12 (CEN 2015) that it can be extended to steels up to grade S700 without further adjustments. The Australian standard AS/NZ 2327 (2017) has also extended its applicability to steels with yield strength up to 690 MPa, referring to AS 4100 (2020) for the variation of the mechanical properties of steel with temperature. Although the range of steel grades is enlarged in ANSI/AISC 360-16 (AISC 2010), its reduction factors apply only to steels up to grade S450. The field of application of the reduction coefficients provided by British Standards BS590-8:2003 (BSI 2003) which is limited to structural steels between grades S275 and S355 is even more restrictive, making them unsuitable for their application to high strength steels assessment in fire conditions.

A deep literature analysis revealed several studies on reduction coefficients at high temperatures involving high strength steels of different grades such as S690 (Qiang *et al.* 2012), Q690 (Li and Song 2020), S700 (Shakil *et al.* 2020) and steels with nominal yield stresses between 700 and 900 MPa (Li and Young 2017). Researchers conducted experimental campaigns to characterize the mechanical properties of these steels under thermal conditions. They proposed reduction factors for key mechanical parameters, such as the elastic modulus, the yield strength, and the ultimate strength. Comparison with the proposals of different established design standards was also presented (Qiang *et al.* 2012, Li and Young 2017). Predictive equations and constitutive models were also developed (Shakil *et al.* 2020; Li and Young 2017), assessing material behaviour under different temperature ranges, and shedding light on the response of high strength steels at elevated

temperatures. Additionally, Hassanein *et al.* (2022) suggested modifying the design codes to adequately predict the strength of S690 steels (Eurocode 3 Part 1.2 (CEN 2005) and AISC (AISC 2010)).

### 5.2 HSC reduction coefficients

The design provisions in EN1992-1-2 (CEN 2004) are applicable to normal weight concrete with characteristic compressive strength up to 90 MPa (cylinder strength), additional rules for concrete with strength above 50 MPa being given in its section 6. For compressive strengths ranging from C55/67 class to C90/105 class, Table 6.1N contains high strength concrete reduction coefficients. In turn, the Australian standard AS/NZ 2327 (2017) refers to EN1992-1-2 (CEN 2004) for the variation of the mechanical properties of concrete with temperature. In North America, the standard ACI 216.1-14 (ACI 2014) offers formulas to predict the behaviour of normal strength concrete at high temperatures. Despite the absence of direct specifications, this code is assumed not to encompass provisions applicable to high strength concrete. Facing the lack of specific guidelines, several researchers have proposed equations and temperature-dependent strength reduction coefficients for HSC (Phan and Carino 2003, Kodur *et al.* 2004, Matsudo *et al.* 2008). Other studies offered tabulated relationships between material properties and temperatures (Aslani and Bastami 2011). It is worth mentioning the extensive analysis performed by Elsanadedy (2019) where a profound analysis of design code provisions on this matter and literature proposals were made to be contrasted to experimental data.

### 5.3 Plastic resistance design equation for SR-CFST stub columns at elevated temperatures

The approach presented in this section for evaluating the plastic resistance of SR-CFST stub columns at elevated temperature is based on dividing the cross-section into five components, with different representative temperatures, see Fig. 17. The embedded steel profile is split into its flanges and web, while the concrete infill is divided into two parts: the concrete encased by the steel profile flanges and the concrete ring between the steel profile and outer tube. This approach aligns with the method proposed by Yang *et al.* (2020) and EN1994-1-2 Annex G (CEN 2005) provisions for partially encased composite columns.

In order to evaluate the mechanical contribution of each part of the section at a certain time period, a representative temperature needs to be obtained, which is subsequently used to reduce the material strength. To perform the assessment of the design equations in this section, these representative temperatures were derived from the experimental thermocouple measurements. The procedure for obtaining the five representative temperatures ( $\theta_i$ ) indicated in Fig. 17 was as follows. The temperature of the outer steel tube ( $\theta_s$ ) was derived by computing the mean value of thermocouples TC1 and TC6, resulting in a range between 650 to 770 °C at failure time. For the steel profile flanges, the corresponding temperature ( $\theta_f$ ) was obtained

Table 3 Average error ( $\xi$ ) obtained for the different HSS proposals assessed

Specimen	EN1993-1-2 (2005)	Qiang <i>et al.</i> (2012)	Li and Young (2017)	Li and Song (2020)	Shakil <i>et al.</i> (2020)	AS4100 (2020)
SR-CFST-C-TM2	0.94	1.07	1.15	1.11	1.12	1.13
SR-CFST-S-TM2	0.93	1.04	1.16	1.13	1.11	1.08
Mean	0.93	1.06	1.15	1.12	1.12	1.10

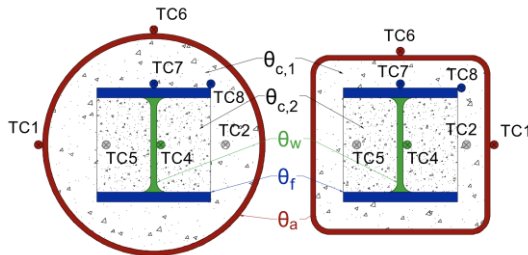


Fig. 17 Sub-division of the cross-section to calculate the plastic resistance at elevated temperatures

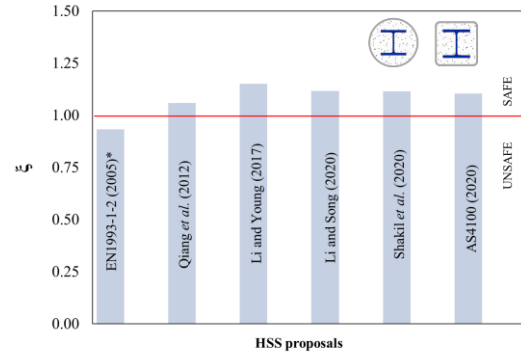
using the average value from thermocouples TC7 and TC8. In turn, the temperature at the web of the embedded steel profile ( $\theta_w$ ) was determined solely by thermocouple TC4. The temperatures recorded at failure time for the inner profile ranged from 410 to 620 °C. Regarding the concrete infill, the representative temperatures for the ring ( $\theta_{c,1}$ ) and for the encased concrete ( $\theta_{c,2}$ ) were given by thermocouples TC2 and TC5 respectively. The temperatures measured within the encased areas of the concrete infill spanned from 420 to 550 °C at failure time, while the ring areas exhibited higher temperatures, ranging between 475 and 620 °C.

Once this simplified temperature field is obtained, the plastic resistance to axial compression of a SR-CFST cross-section in case of fire ( $N_{pl,Rd,fi}$ ) can be computed by adapting the equation given in Clause 4.3.5.1(4) of EN1994-1-2 (CEN 2005) for composite columns, as proposed in Eq. (3). To consider the inner steel profile, its contribution is added in the summation as proposed by Liew and Xiong (2015). Note that the area of the inner steel profile flanges ( $A_f$ ) and web ( $A_w$ ) has been split in this equation to consider their degradation with temperature separately, as well as the concrete infill, which has been divided into the two zones mentioned above: the concrete ring ( $A_{c,1}$ ) and the encased concrete ( $A_{c,2}$ ).

$$N_{pl,Rd,fi} = A_a \cdot f_y(\theta_a) + A_{c,1} \cdot f_c(\theta_{c,1}) + A_{c,2} \cdot f_c(\theta_{c,2}) + A_w \cdot f_y(\theta_w) + 2 \cdot A_f \cdot f_y(\theta_f) \quad (3)$$

Eq. (3) was used to calculate the value of  $N_{pl,Rd,fi}$  obtained when different sets of reductions coefficients for the high performance materials were applied ( $N_{pred}$  for each case). Various proposals were assessed comparing their prediction with the experimental results of the conducted tests.

The experimentally applied load ( $N_{exp}$ ) was compared to the calculated cross-sectional resistance ( $N_{pred}$ ) at the highest recorded temperatures by computing the error  $\xi$ , defined as given in Eq. (4):



\*As per Clause 2.2 of EN1993-1-12 (CEN 2015): “The standard is applicable to steels with grades greater than S460 up to S700 without further additional rules.

Fig. 18 Predictions for columns SR-CFST-C-TM2 and SR-CFST-S-TM2 using different HSS proposals

$$\xi = \frac{N_{exp}}{N_{pred}} \quad (4)$$

#### High strength steel proposals

Using the values proposed for the reduction coefficients of high strength steels in the works commented above (Qiang *et al.* 2012, Li and Song 2020, Shakil *et al.* 2020, and Li and Young 2017), the predicted resistances are calculated and compared with the experimental loads.

The different high strength steel proposals were evaluated using specimens with HSS inner profiles and NSC (i.e., SR-CFST-S-TM2 and SR-CFST-C-TM2) to ensure a meaningful comparison. The results are summarised in the bar graph presented in Fig. 18 and in Table 3.

Note that a value of the average error  $\xi$  greater than one means that the proposal of reduction coefficients evaluated is safe in comparison with the experimental result - i.e., the value of the predicted cross-sectional resistance to compression of the SR-CFST column at elevated temperatures ( $N_{pred}$ ) is less than the experimental load -.

From this comparison, it can be seen that the most accurate model from the literature is that proposed by Qiang *et al.* (2012), exhibiting deviations of about 6% from the experimental results. The models proposed by Li and Song (2020) and Shakil *et al.* (2020) lead to conservative predictions with a 12% deviation from the experimental values, while the proposal by Li and Young (2017) shows the lower agreement (15% deviation), although with conservative predictions.

The reduction coefficients in EN1993-1-2 (CEN 2005)

Table 4 Average error ( $\xi$ ) obtained for the different HSC proposals assessed

Specimen	Phan and Carino (2003)	EN1992-1-2 Table 6.1N (2004)	Kodur <i>et al.</i> (2004)	Matsudo <i>et al.</i> (2008)	Aslani and Bastami (2011)
SR-CFST-C-TM3	1.16	1.00	0.99	1.21	1.02
SR-CFST-S-TM3	1.22	1.04	1.03	1.17	1.07
Mean	1.19	1.02	1.01	1.19	1.04

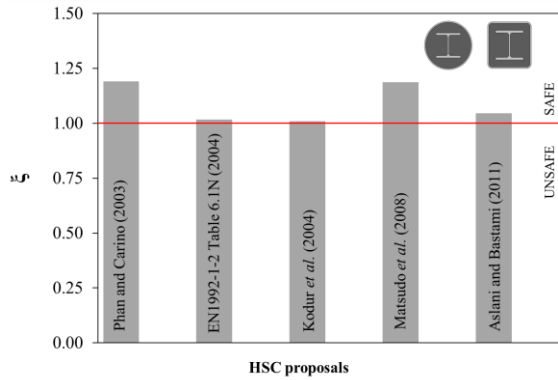


Fig. 19 Predictions for columns SR-CFST-C-TM3 and SR-CFST-S-TM3 using different HSC proposals

have also been included in this comparison, showing non-conservative predictions as compared to the experimental results, with a 7% overestimation. This may be due to a lack of calibration of the design code for this range of strengths, as the reduction coefficients are specifically derived for steel grades up to 460 MPa, although extended to 700 MPa as per Clause 2.2 of EN1993-1-12 (CEN 2015). Also the steel yield strength reduction proposal at elevated temperatures from AS4100 (2020) has been included in this comparison, showing conservative results, with an average error of 10%.

#### High strength concrete proposals

An identical procedure is applied in this section for the evaluation of the HSC proposals in the prediction of the cross-sectional resistance to compression of the SR-CFST columns at elevated temperatures. The different proposals were examined by using the appropriate test specimens for comparison (i.e., SR-CFST-S-TM3 and SR-CFST-C-TM3), see Fig. 19 and Table 4.

The HSC strength reduction coefficient proposals with temperature by Phan and Carino (2003), EN1992-1-2 (CEN 2004), Kodur *et al.* (2004), Matsudo *et al.* (2008), and Aslani and Bastami (2011) were studied.

As it can be seen in Fig. 19 and Table 4, the coefficients from Table 6.1N of EN1992-1-2 (CEN 2004), along with the models proposed by Kodur *et al.* (2004) and Aslani and Bastami (2011), demonstrate a significant accuracy in predicting the behaviour of the high strength concrete core with average errors of 1.02, 1.01 and 1.04 (lower than a 5% deviation), all of them lying on the safe side.

In turn, the reduction coefficients proposed by Phan and Carino (2003) and Matsudo *et al.* (2008) provide considerably conservative predictions, both with a deviation of a 19% from the actual column capacity at high

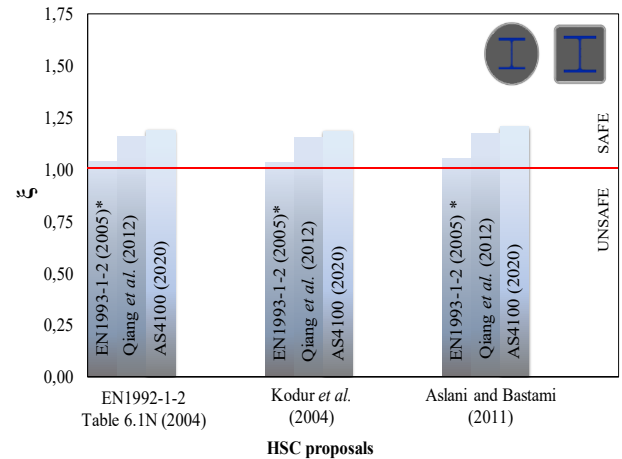


Fig. 20 Predictions for columns SR-CFST-C-TM4 and SR-CFST-S-TM4 combining HSS and HSC proposals

temperatures.

As can be observed, none of the proposals analysed provided unsafe predictions, which means that none of them overestimated the cross-sectional resistance to compression of the SR-CFST column at elevated temperatures.

#### Combination of proposals

Finally, a third comparison is conducted, using the insights gained from the HSS and HSC models studied in the previous sections. The best performing reduction coefficients for each material are selected (those not exceeding a 10% error in the previous evaluations) and compared against the experimental tests that make use of both HSS and HSC (test specimens SR-CFST-S-TM4 and SR-CFST-C-TM4). The results for this comparison can be observed in Fig. 20 and Table 5.

The aim of this analysis is to determine which combination is the most suitable to predict the cross-sectional resistance to compression of SR-CFST columns at high temperatures according to the experimental results presented above by the authors. For HSS, the proposals considered are the reduction coefficients from EN1993-1-2 (CEN 2005), as well as those by Qiang *et al.* (2012) and AS4100 (2020). In turn, for HSC, the selected proposals include the reduction coefficients from EN1992-1-2 (CEN 2004) and those by Kodur *et al.* (2004), and Aslani and Bastami (2011).

As can be seen in Fig. 20 and Table 5, irrespective of the HSC proposal employed, the three selected options for HSS result in conservative predictions, with average values above one. However, the best agreement between the predicted and the tested failure loads at elevated

Table 5 Average error ( $\zeta$ ) obtained for the combined HSS and HSC proposals assessed

Specimen	EN1992-1-2 (2004)			Kodur <i>et al.</i> (2004)			Aslani and Bastami (2011)		
	EN1993-1-2 (2005)	Qiang <i>et al.</i> (2012)	AS4100 (2020)	EN1993-1-2 (2005)	Qiang <i>et al.</i> (2012)	AS4100 (2020)	EN1993-1-2 (2005)	Qiang <i>et al.</i> (2012)	AS4100 (2020)
SR-CFST-C-TM4	1.06	1.18	1.22	1.05	1.17	1.21	1.17	1.19	1.23
SR-CFST-S-TM4	1.02	1.14	1.16	1.02	1.14	1.16	1.03	1.15	1.18
Mean	1.04	1.16	1.19	1.04	1.15	1.18	1.05	1.17	1.20

temperatures is obtained when combining the reduction coefficients for HSC from Table 6.1N of EN1992-1-2 (CEN 2004) and those for HSS in EN1993-1-2 (CEN 2005), with an average error of 1.04. Also the reduction coefficients proposed by Kodur *et al.* (2004) or Aslami and Bastami (2011), combined with EN1993-1-2 (CEN 2005), demonstrate a good agreement with the test results. The reduction coefficients for HSS proposed by Qiang *et al.* (2012) provide errors above a 15% when combined with the studied reduction coefficients for HSC, although they lay on the safe side. Finally, the provisions in AS4100 (2020) for the reduction of steel strength with temperature also result in safe predictions, although too safe-sided, with an error of about a 20%.

It should be noted that the present comparison is in its initial stages, relying on a limited number of experiments. Conclusions should be cautiously approached, as further research and validation are necessary to ensure sufficient accuracy. Additional experiments and extension to validated numerical models, accompanied by comprehensive parametric studies, are required for a reliable analysis before drawing firm conclusions that can lead to the development of design recommendations.

## 6. Conclusions

In this paper, the thermo-mechanical response of SR-CFST stub columns has been studied through the experimental investigation here described. The evolution of the cross-sectional temperatures with time and the axial displacement versus time histories were analysed. Ten SR-CFST specimens, four circular and six square, were tested together with two hollow steel tubes which served as reference. First, the columns were loaded at a certain load level and afterwards uniformly heated inside an electric furnace until failure. According to their external shape, eight of the columns were grouped into two series comprising circular and square geometries respectively (TM1-TM4) combining normal with high performance materials for the inner components (concrete infill and embedded steel profile). For the sake of comparison, the selected circular and square steel tubes had a comparable steel usage. Two of the square SR-CFST columns (TM5 and TM6) had high strength steel in the outer tube. From the results of the thermo-mechanical tests, some conclusions can be drawn:

- Temperatures were generally higher for the square SR-CFST columns than for the corresponding circular columns,

which may be due to the effect of the higher section factor of square columns as compared to their circular counterparts.

- The circular specimens reached higher failure times than the square columns. The failure time significantly increased with the use of high strength steel at the embedded steel profile, as well as with the use of high strength concrete as infill.

- From the fire design point of view, it is not worth to use neither a high amount of steel, nor a high steel grade at the outer tube.

The current design provisions for the evaluation of the cross-sectional plastic resistance of SR-CFST columns at elevated temperatures and the applicability of the currently available strength reduction coefficients for HSS and HSC from the design codes and the reviewed literature was assessed, by contrast with the experimental results. It was found that the strength reduction coefficients from the Eurocodes – EN1992-1-2 (CEN 2004) and EN1993-1-2 (CEN 2005) – provide the more accurate results in predicting the axial capacity at elevated temperatures of SR-CFST stub columns with high performance materials, followed by the proposal from Qiang *et al.* (2012) and the provisions in the Australian code AS4100 (2020), all of them leading to conservative results.

In the framework of the nationally funded project that overarches the present research (HIFICOMP) the authors will carry out further experimental tests and numerical studies to extend the conclusions drawn in this work and to be able to develop fire design recommendations for the use of high performance materials in SR-CFST columns.

## Acknowledgments

The authors would like to express their sincere gratitude for the help provided through the Grant PID2019-105908RB-I00 and for the first author's pre-doctoral contract through the Grant PRE2020-093106 funded by MCIN/AEI/ 10.13039/501100011033 and by "ESF Investing in your future". The authors are deeply grateful to Dr Enrique Serra for his help in preparing the test specimens, and to Dr Andrés Lapuebla-Ferri and Dr David Pons for their help in conducting the material tests. Finally, the authors would like to acknowledge the funding for open access charge from CRUE-Universitat Politècnica de València.

## References

- ACI 216.1-14 (2014), *Code Requirements for Determining Fire Resistance of Concrete and Masonry Construction Assemblies*, American Concrete Institute; Farmington Hills, MI, USA.
- ANSI/AISC 360-16 (2010), *Specification for Structural Steel Buildings*, American Institute of Steel Construction; Chicago, IL, USA.
- AS 4100 (2020), *Steel structures*, Standards Australia Ltd.; Sydney, Australia.
- AS/NZS 2327 (2017), *Composite structures - Composite steel-concrete construction in buildings*, Standards Australia/Standards New Zealand; Auckland, New Zealand.
- Aslani, F. and Bastami, M. (2011), "Constitutive relationships for normal-and high-strength concrete at elevated temperatures" *ACI Mater. J.*, **108**(4), 355-364. <https://doi.org/10.14359/51683106>.
- BS 5950-8 (2003), *Structural Use of Steelwork in Building Part 8: Code of Practice for Fire Resistant Design*, British Standards Institution; London, UK.
- Dotreppe, J.C., Chu, T.B. and Franssen, J.M. (2010), "Steel hollow columns filled with self-compacting concrete under fire conditions." *Proceedings of the 3rd Congress of the International Federation for Structural Concrete (FIB) and PCI Conference*, Washington D.C., May.
- Elsanadedy, H.M. (2019), "Residual Compressive Strength of High-Strength Concrete Exposed to Elevated Temperatures", *Adv. Mater. Sci. Eng.*, **2019**, 6039571. <https://doi.org/10.1155/2019/6039571>
- EN1363-1:2020 (2020), *Fire Resistance Tests - Part 1: General Requirements*, CEN European Committee for Standardization, Brussels, Belgium.
- EN1992-1-2 (2004), *Eurocode 2: Design of Concrete Structures, Part 1.2: General rules - Structural Fire Design*, CEN European Committee for Standardization; Brussels, Belgium.
- EN1993-1-2 (2005), *Design of Steel Structures, Part 1.2: General Rules - Structural Fire Design*, CEN European Committee for Standardization; Brussels, Belgium.
- EN1994-1-1 (2004), *Eurocode 4: Design of Composite Steel and Concrete Structures. Part 1.1: General rules and rules for buildings*, European Committee for Standardization; Brussels, Belgium.
- EN1994-1-2 (2005), *Eurocode 4: Design of Composite Steel and Concrete Structures. Part 1.2: General rules - Structural fire design*, European Committee for Standardization; Brussels, Belgium.
- EN1993-1-12 (2015), *Design of Steel Structures, Part 1-12: Additional Rules for the Extension of EN 1993 up to Steel Grades S700*, CEN European Committee for Standardization; Brussels, Belgium
- Espinós, A., Romero, M.L. and Lam, D. (2016), "Fire performance of innovative steel-concrete composite columns using high strength steels", *Thin-Wall. Struct.*, **106**, 113-128. <https://doi.org/10.1016/j.tws.2016.04.014>.
- Hassanein, M.F., Zhang, Y.M., Shao, Y.B. and Zhou, M. (2022), "New AISC and EC3 design for S690 plate girders at elevated temperatures" *J. Constr. Steel Res.*, **194**, 107313. <https://doi.org/10.1016/j.jcsr.2022.107313>
- ISO 12570:2000 (2000), *Hygrothermal performance of building materials and products - Determination of moisture content by drying at elevated temperature*, International Organization for Standardization, Geneva, Switzerland.
- Kodur, V.K.R., Wang, T.C. and Cheng, F.P. (2004), "Predicting the fire resistance behaviour of high strength concrete columns", *Cem. Concr. Compos.*, **26**(2), 141-153. [https://doi.org/10.1016/S0958-9465\(03\)00089-1](https://doi.org/10.1016/S0958-9465(03)00089-1).
- Li, G.Q. and Song, L.X. (2020), "Mechanical properties of TMCP Q690 high strength structural steel at elevated temperatures", *Fire Saf. J.*, **116**, 103190. <https://doi.org/10.1016/j.firesaf.2020.103190>
- Li, H.T. and Young, B. (2017), "Material properties of cold-formed high strength steel at elevated temperatures", *Thin-Wall. Struct.*, **115**, 289-299. <https://doi.org/10.1016/j.tws.2017.02.019>.
- Liew, J.Y.R. and Xiong, M. (2015), *Design Guide for Concrete Filled Tubular Members with High Strength Materials to Eurocode 4*, Research Publishing, Singapore, Republic of Singapore.
- Mao, W.J., Wang, W. and Zhou, K. (2022), "Fire performance on steel-reinforced concrete-filled steel tubular columns with fire protection", *J. Constr. Steel Res.*, **199**, 107580. <https://doi.org/10.1016/j.jcsr.2022.107580>
- Mao, W.J., Wang, W., Zhou, K. and Du, E.F. (2021), "Experimental study on steel-reinforced concrete-filled steel tubular columns under the fire", *J. Constr. Steel Res.*, **185**, 106867. <https://doi.org/10.1016/j.jcsr.2021.106867>
- Mao, W.J., Zhou, K. and Wang, W. (2023), "Investigation on fire resistance of steel-reinforced concrete-filled steel tubular columns subjected to non-uniform fire", *Eng. Struct.*, **280**, 115653. <https://doi.org/10.1016/j.engstruct.2023.115653>
- Matsudo, M., Nishida, H., Ohtsuka, T., Hirashima, T. and Abe, T. (2008), "mechanical properties of high strength concrete at high temperatures", *J. Struct. Construct. Eng. Transact. AIJ*, **73**(624), 341-347. <https://doi.org/10.3130/aajs.73.341>.
- Medall, M., Espinós, A., Albero, V. and Romero, M.L. (2022), "Simplified proposal for the temperature field of steel-reinforced CFST columns exposed to fire", *Eng. Struct.*, **273**, 115083. <https://doi.org/10.1016/j.engstruct.2022.115083>.
- Meng, F.Q., Zhu, M.C., Clifton, G.C., Ukanwa, K.U. and Lim, J.B.P. (2020), "Performance of square steel-reinforced concrete-filled steel tubular columns subject to non-uniform fire", *J. Construct. Steel Res.*, **166**, 105909. <https://doi.org/10.1016/j.jcsr.2019.105909>.
- Meng, F-Q., Zhu, M-C., Clifton, G.C., Ukanwa, K.U. and Lim, J.B.P. (2021), "Fire performance of edge and interior circular steel-reinforced concrete-filled steel tubular stub columns", *Steel Compos. Struct.*, **41**(1), 115-122. <https://doi.org/10.12989/scs.2021.41.1.115>
- Phan, L.T. and Carino, N.J. (2006), "Code provisions for high strength concrete strength-temperature relationship at elevated temperatures", *Mater. Struct.*, **36**(256), 91-98. <https://doi.org/10.1007/BF02479522>.
- Pons, D., Espinós, A., Albero, V. and Romero, M.L. (2018), "Numerical study on axially loaded ultra-high strength concrete-filled dual steel columns", *Steel Compos. Struct.*, **26**(6), 705-717. <https://doi.org/10.12989/scs.2018.26.6.705>.
- Qiang, X., Bijlaard, F. and Kolstein, H. (2012), "Dependence of mechanical properties of high strength steel S690 on elevated temperatures", *Construct. Build. Mater.*, **30**, 73-79. <https://doi.org/10.1016/j.conbuildmat.2011.12.018>.
- Romero, M.L., Espinós, A., Portolés, J.M., Hospitaler, A. and Ibáñez, C. (2015), "Slender double-tube ultra-high strength concrete-filled tubular columns under ambient temperature and fire", *Eng. Struct.*, **99**, 536-545. <http://dx.doi.org/10.1016/j.engstruct.2015.05.026>.
- Shakil, S., Lu, W. and Puttonen, J. (2020), "Experimental studies on mechanical properties of S700 MC steel at elevated temperatures", *Fire Saf. J.*, **116**, 103157. <https://doi.org/10.1016/j.firesaf.2020.103157>.
- Yang, X., Tang, C., Chen, Y. and Qiao, T.Y. (2020), "Compressive behavior of steel-reinforced concrete-filled square steel tubular stub columns after exposure to elevated temperature", *Eng. Struct.*, **204**. <https://doi.org/10.1016/j.engstruct.2019.110048>.